Matter and Radiation at Extremes | RESEARCH ARTICLE | scitation.org/journal/mre

Generation of high intensity speckles in overlapping laser beams

Cite as: Matter Radiat. Extremes 8, 025903 (2023); doi: 10.1063/5.0123585
Submitted: 31 August 2022 • Accepted: 22 January 2023 •
Published Online: 21 February 2023

Liang Hao, Jie Qiu, and Wen Yi Huo[a)]

AFFILIATIONS

Laboratory of Computational Physics, Institute of Applied Physics and Computational Mathematics, Beijing 100094, China

[a)]Author to whom correspondence should be addressed: huo_wenyi@iapcm.ac.cn

ABSTRACT

A new mechanism for the generation of high intensity speckles by coupling of overlapping beams is discovered and studied in detail. Using three-dimensional simulations, the coupling of overlapping beams smoothed by phase plates and by polarization smoothing are investigated in the regime relevant to inertial confinement fusion studies. It is found that the intensity distribution of the laser beam spot can be changed by nonuniform spatial phase modulation, and the speckles formed by the phase plate can be split into smaller speckles with higher intensities, which is favorable for the generation of laser plasma instabilities. Stimulated Brillouin scattering is compared in simulations with and without coupling of the overlapping incident beams, and the results confirm the enhancement of stimulated Brillouin scattering due to this mechanism.

I. INTRODUCTION

In laser-driven inertial confinement fusion (ICF), owing to the energy limitations of individual laser beams and the requirement of symmetrical driving, multiple laser beams are used to drive the target.[1,2] For direct-drive ICF, the laser beams overlap in the underdense coronal plasma ablated from the capsule. For indirect-drive ICF, the laser beams overlap near the laser entrance hole and in the filled gas inside the hohlraum. In these regions, many laser–plasma instabilities (LPIs) can be stimulated or amplified by the overlapping beams, such as crossed-beam energy transfer (CBET),[3–7] stimulated Brillouin scattering (SBS),[8–11] stimulated Raman scattering (SRS),[12–18] and two-plasmon decay (TPD).[19,20] For indirect-drive hohlraums, CBET is usually used as an important symmetry tuning method,[4–6] although it is considered to be a crucial energy loss mechanism in the case of direct-drive ICF.[7] Besides, the scattered light from SBS and SRS will take some energy away from the target and reduce the laser energy absorption, and the hot electrons generated from SRS and TPD may preheat the fuel. Although a 1.35 MJ fusion energy has been achieved at the National Ignition Facility (NIF),[21,22] LPIs are still important issues and need to be well controlled to improve energy absorption efficiency and radiation symmetry.

To reduce LPI, laser beam smoothing techniques, such as phase plates,[23–25] smoothing by spectral dispersion (SSD),[26] and polarization smoothing (PS),[27] have been applied in experiments. Recently, some new theoretical schemes, such as spike trains of uneven duration and delay,[28] polarization rotation,[29] broadband lasers,[30,31] time-dependent polarization rotation via pulse chirping,[32] and sunlight-like lasers[33] have been proposed. A dynamic stabilization method[34] has also been studied with the aim of controlling perturbation growth of filamentation by wobbler or driver oscillation.[35] In addition, a low-coherence laser facility with kilojoule energy output has been demonstrated experimentally.[36] To control energy transfer in indirect-drive hohlraums, wavelength separation has been added among beam quads with different incident angles on the NIF,[5] because energy transfer is highly dependent on the wavelength separation between the two overlapping beams. In reality, under the ponderomotive force of the two overlapping beams, a plasma grating can be generated. When the phase velocity of the grating is equal to the sound speed in the reference frame of the plasma, the amplitudes of the laser beams can be modified most efficiently.[37] Even when the overlapping beams have the same frequency, their phases can still be modulated by three-wave coupling. Therefore, control through the use of a plasma grating is also adopted in the design of plasma-based photonic devices.[38,39] However, previous theoretical studies of phase modulation between overlapping beams have been limited because of their use of the plane wave assumption without consideration of the beam

smoothing effect. In this paper, the interaction of overlapping beams smoothed by phase plates and polarization smoothing is investigated using a three-dimensional code of overlapping laser–plasma instabilities (COLA). We find a new generation mechanism for high intensity speckles in the overlapping beams. This mechanism increases the portion of high intensity within the beam spots, and worsens the quality of the laser beams, which will result in stronger LPIs. The SBS in the overlapping beams is taken as an example demonstrating the enhancement of LPIs by this mechanism.

II. PHYSICAL MODEL

To study the LPIs stimulated by multiple overlapping laser beams, we employ the three dimensional steady-state code COLA, which is currently used to study coupling processes of different beams, including CBET and phase modulation as well as SBS, under conditions in which the beams are smoothed by phase plates and polarization smoothing. COLA solves the equations for the vector potentials of light waves, including the laser light and the scattered light from SBS, and the equations for the electron density perturbations generated by the beating of the different waves. In this section, we introduce the physical basis of COLA in detail.

In COLA, the laser beams are assumed to propagate mainly along the $\hat{z}$ direction, and the vector potential of the light wave of laser beam α is defined as

$$\vec{A}_\alpha = \left(\frac{1}{2}A_{\alpha x}e^{i\Psi_\alpha} + \text{c.c.}\right)\vec{e}_x + \left(\frac{1}{2}A_{\alpha y}e^{i\Psi_\alpha} + \text{c.c.}\right)\vec{e}_y, \tag{1}$$

where $A_{\alpha x}$ and $A_{\alpha y}$ are the slowly varying complex amplitudes of the two orthogonal polarization components of $\vec{A}$, and Ψ_α is the rapidly varying phase. The frequency of beam α is $\omega_\alpha = -\partial_t\Psi_\alpha$ and its wavenumber $k_\alpha = \partial_z\Psi_\alpha$. Similarly, the vector potential of the SBS scattered light is given by

$$\vec{A}_B = \left(\frac{1}{2}A_{Bx}e^{i\Psi_B} + \text{c.c.}\right)\vec{e}_x + \left(\frac{1}{2}A_{By}e^{i\Psi_B} + \text{c.c.}\right)\vec{e}_y, \tag{2}$$

where A_{Bx} and A_{By} are the slowly varying complex amplitudes of $\vec{A}_B$ in the $\hat{x}$ and $\hat{y}$ directions and Ψ_B is its rapidly varying phase. The frequency and wavenumber of the SBS scattered light are $\omega_B = -\partial_t\Psi_B$ and $k_B = \partial_z\Psi_B$, respectively. The perturbation of the electron density n_e is given by

$$\delta n = \delta n_\perp + \frac{1}{2}\sum_{\alpha\neq\beta}\left(\delta n_{\alpha\beta}e^{i(\Psi_\alpha-\Psi_\beta)} + \text{c.c.}\right) + \frac{1}{2}\sum_\alpha\left(\delta n_\alpha^B e^{i(\Psi_\alpha-\Psi_B)} + \text{c.c.}\right), \tag{3}$$

where $\delta n_\perp(z) = n_e(x,y,z) - \langle n_e(x,y,z)\rangle_{x,y}$ denotes the transverse nonuniformity of the electron density on the plane perpendicular to the $\hat{z}$ axis, $\delta n_{\alpha\beta}$ is the slowly varying complex amplitude of the density perturbation generated by the beating of the overlapping beams α and β, and δn_α^B is the slowly varying complex amplitude of the density perturbation generated by the beating of beam α and the SBS scattered light. Under the envelope and paraxial approximations,[40] the steady-state equations for the incident light can be derived from the Maxwell equations as

$$\left(\frac{\partial}{\partial z} + \frac{\nu_\alpha}{v_{g\alpha}} + \frac{\partial k_\alpha}{2k_\alpha\partial z} - \frac{i\nabla_\perp^2}{2k_\alpha} + \frac{i\omega_{pe}^2}{2k_\alpha c^2}\frac{\delta n_\perp}{n_e}\right)A_{\alpha x} = -\frac{i\omega_{pe}^2}{4n_e k_\alpha c^2}\left(\sum_{\beta\neq\alpha}\delta n_{\alpha\beta}A_{\beta x} + \delta n_\alpha^B A_{Bx}\right) \tag{4}$$

and

$$\left(\frac{\partial}{\partial z} + \frac{\nu_\alpha}{v_{g\alpha}} + \frac{\partial k_\alpha}{2k_\alpha\partial z} - \frac{i\nabla_\perp^2}{2k_\alpha} + \frac{i\omega_{pe}^2}{2k_\alpha c^2}\frac{\delta n_\perp}{n_e}\right)A_{\alpha y} = -\frac{i\omega_{pe}^2}{4n_e k_\alpha c^2}\left(\sum_{\beta\neq\alpha}\delta n_{\alpha\beta}A_{\beta y} + \delta n_\alpha^B A_{By}\right), \tag{5}$$

where ω_{pe} and c are the electron plasma frequency and the speed of light in vacuum, and $v_{g\alpha}$ and ν_α are the group velocity and collisional absorption rate, respectively, of beam α. Similarly, the equations for the SBS scattered light can be written as

$$\left(\frac{\partial}{\partial z} - \frac{\nu_B}{v_{gB}} + \frac{\partial k_B}{2k_B\partial z} + \frac{i\nabla_\perp^2}{2k_B} - \frac{i\omega_{pe}^2}{2k_B c^2}\frac{\delta n_\perp}{n_e}\right)A_{Bx} = \frac{i\omega_{pe}^2}{4n_e k_B c^2}\sum_\alpha \delta n_\alpha^{B*}A_{\alpha x} \tag{6}$$

and

$$\left(\frac{\partial}{\partial z} - \frac{\nu_B}{v_{gB}} + \frac{\partial k_B}{2k_B\partial z} + \frac{i\nabla_\perp^2}{2k_B} - \frac{i\omega_{pe}^2}{2k_B c^2}\frac{\delta n_\perp}{n_e}\right)A_{By} = \frac{i\omega_{pe}^2}{4n_e k_B c^2}\sum_\alpha \delta n_\alpha^{B*}A_{\alpha y}, \tag{7}$$

where v_{gB} and ν_B are the group velocity and collisional absorption rate, respectively, of the SBS scattered light. The expressions for the enveloped density perturbations are

$$\delta n_{\alpha\beta} = -K\frac{(k_\alpha - k_\beta)^2}{8\pi m_e c^2}\left(A_{\alpha x}A_{\beta x}^* + A_{\alpha y}A_{\beta y}^*\right) \tag{8}$$

and

$$\delta n_\alpha^B = -K\frac{(k_\alpha - k_B)^2}{8\pi m_e c^2}\left(A_{\alpha x}A_{Bx}^* + A_{\alpha y}A_{By}^*\right), \tag{9}$$

where $K = \chi_e(1+\chi_i)/(1+\chi_e+\chi_i)$ is the plasma coupling coefficient and m_e is the electron mass. Here, $\chi_e = Z'[\omega/k(\sqrt{2}v_{Te})]/(k\lambda_{De})^2/2$ and $\chi_i = \sum_j Z'[\omega/k(\sqrt{2}v_{Tj})]/(k\lambda_{Dj})^2/2$ are the electron and ion susceptibilities, respectively, which are functions of the frequency ω and wavenumber k of the different beat waves.[38] $Z(\zeta) = i\sqrt{\pi}e^{-\zeta^2}erfc(-i\zeta)$ is the plasma dispersion function[41] and $erfc(\cdot)$

TABLE I. Simulations of propagation of two overlapping beams.

Case	Laser condition	Switch of coupling
I	CPP in same polarization	Off
II	CPP in same polarization	On
III	CPP in different polarization	On
IV	CPP + PS	On

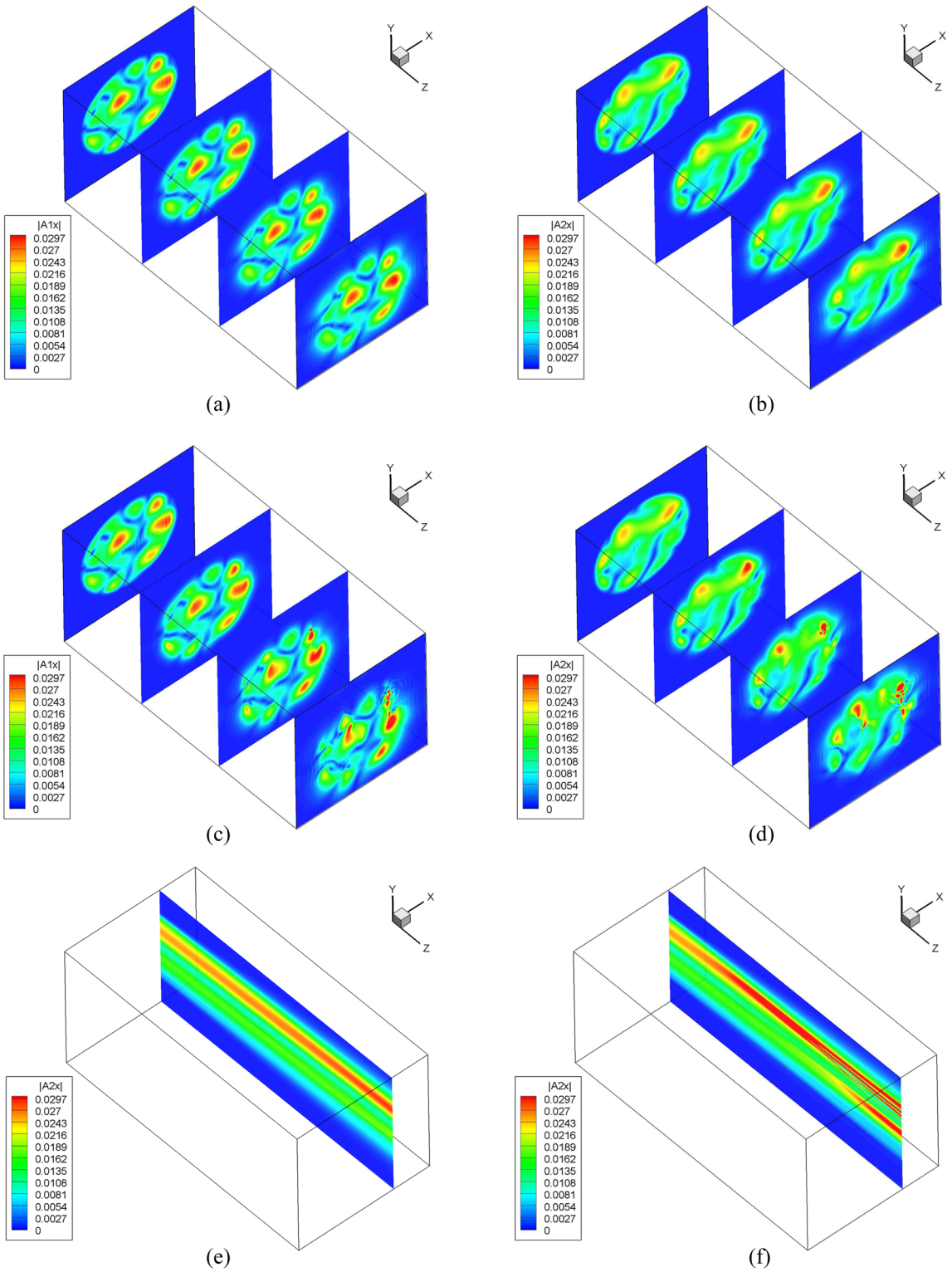

FIG. 1. (a)–(d) Normalized absolute amplitude of the vector potential on different slices in the $\hat{x}$–$\hat{y}$ plane at $z = 0\lambda_c$, $170\lambda_c$, $340\lambda_c$, and $512\lambda_c$ for beams 1 [(a) and (c)] and 2 [(b) and (d)] in cases I [(a) and (b)] and II [(c) and (d)]. (e) and (f) Normalized absolute amplitude of the vector potential on a slice in the $\hat{y}$–$\hat{z}$ plane at $x = 185\lambda_c$ for beam 2 in cases I and II, respectively.

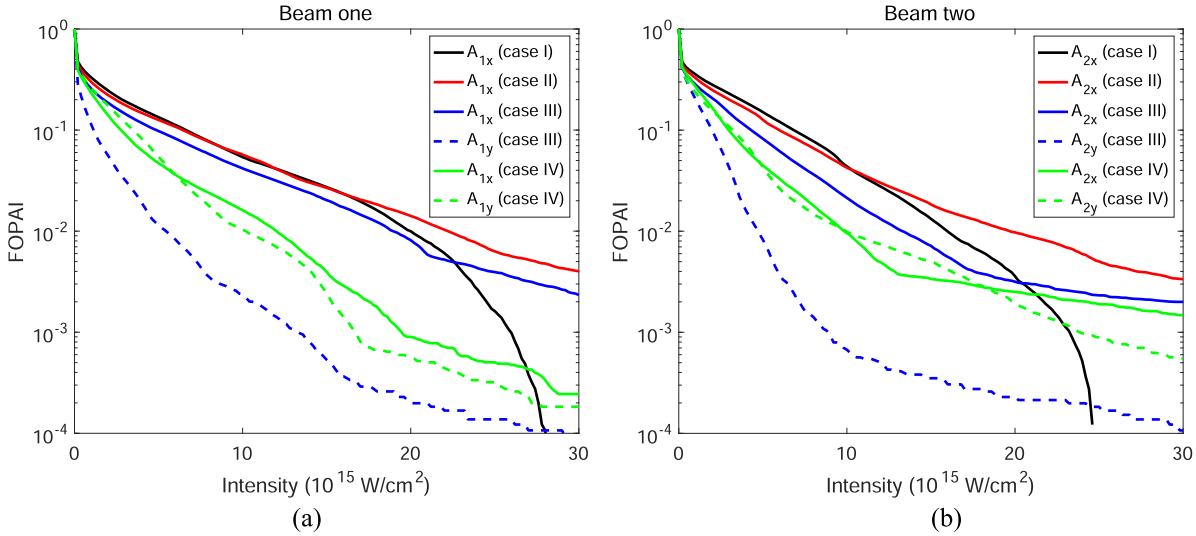

FIG. 2. (a) and (b) FOPAI of beams 1 and 2, respectively, diagnosed in the outgoing $\hat{x}$–$\hat{y}$ plane in the different cases listed in Table I. Solid and dashed lines denote the polarization components in the x and y directions, respectively.

is the complementary error function. v_{Te} and v_{Tj} are the thermal velocities of the electrons and the jth ion species, respectively, and λ_{De} and λ_{Dj} are the corresponding Debye lengths. Using Eqs. (4)–(9), it is possible to directly simulate the coupling among arbitrary laser beams smoothed by phase plates and polarization smoothing and with incident angles less than 10°, as well as the convective growth of the SBS stimulated by these beams.

III. GENERATION OF HIGH INTENSITY SPECKLES BY COUPLING OF OVERLAPPING BEAMS

In the overlapping region of two beams, the phase of each beam can be modified by the other owing to the coupling between them. In this section, to show the influence of nonuniform phase modulation on the overlapping beams clearly without energy transfer between them, the propagation of two overlapping beams with the same wavelength $\lambda_c = 351$ nm is simulated under different laser conditions as listed in Table I. The flow velocity of the plasma, which can induce a Doppler shift in frequency and energy transfer, is set to zero in the simulations. First, cases I (without coupling) and II (with coupling) are compared for two beams smoothed by a continuous phase plate (CPP) with the polarization of the vector potential in the x direction. Then, to study the influence of polarization, case III (with coupling) is considered, with the polarization of beam 2 set along 45° in the $\hat{x}$–$\hat{y}$ plane. In case IV (with coupling), the two beams are smoothed by both a CPP and PS to investigate the effect of PS. Adopting typical plasma parameters near a laser entrance hole,[42] in all simulations in this work, the electron density is chosen as $0.06n_c$, with n_c the critical density, and the temperatures as 1.3 keV for electrons and 0.5 keV for ions. The ion species is fully ionized C_5H_{12}. Owing to the limitations of computational resources, the volume of the simulation box is set as $256\lambda_c \times 256\lambda_c \times 512\lambda_c$. Two overlapping smoothed beams with crossing angle about 5° are launched at the incident $\hat{x}$–$\hat{y}$ plane ($z = 0$) which is also the focal plane of both of the beams. The incident angles of beams 1 and 2 are −2.5° and 2.5°, respectively, from the $\hat{z}$ axis in the y direction. The diameter of the laser spot is $180\lambda_c$, with a tenth-order super-Gaussian distribution. The small crossing angle allows nearly complete overlap of the smoothed beams in the whole simulation domain, and this collinear overlapping corresponds to the experimental situation of the laser quadruplet used on some laser facilities.[19,43] The average intensity of each smoothed beam is $\bar{I} = 2 \times 10^{15}$ W/cm^2.

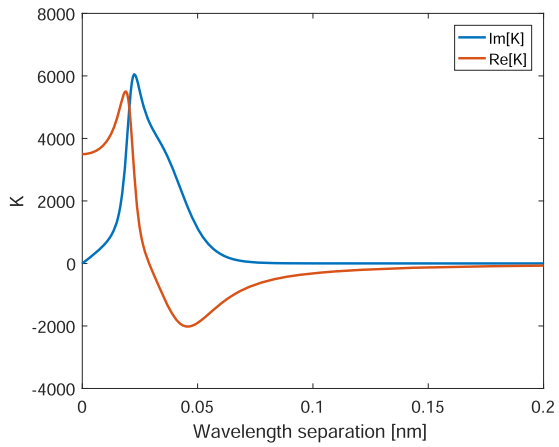

FIG. 3. Real and imaginary parts (orange and blue lines, respectively) of the plasma coupling coefficient K vs the wavelength separation between two beams when the plasma flow velocity is zero.

Figures 1(a) and 1(b) show the speckles on different slices in the $\hat{x}$–$\hat{y}$ plane for beams 1 and 2, respectively, in case I, in which the coupling between the two overlapping beams is turned off. For comparison, the coupling effect is considered in case II, and the

corresponding two beams are presented in Figs. 1(c) and 1(d). The amplitude of beam 2 on a slice in the $\hat{y}$–$\hat{z}$ plane at $x = 185\lambda_c$ is also compared in Figs. 1(e) and 1(f) for cases I and II, respectively. The color map shows the absolute amplitude of the vector potential normalized by $m_e c^2/e$, where m_e and e are the electron mass and charge, respectively. It can be seen that the differences in the intensity distribution on the $\hat{x}$–$\hat{y}$ plane between cases I and II become more and more obvious as the beams propagate along the $\hat{z}$ direction. With regard to the coupling of the laser beams, the distribution of the high intensity speckles is obviously changed, and some new speckles with higher intensity appear in the outgoing $\hat{x}$–$\hat{y}$ plane at $z = 512\lambda_c$ for both beams. In Fig. 2, we present the fractional power above the intensity (FOPAI) of the two beams diagnosed in the outgoing $\hat{x}$–$\hat{y}$ plane. It is clear that the fraction of high intensity up to $(2–3) \times 10^{16}$ W/cm^2 within the beam spots in case II is much higher than that in case I, which means that the beam coupling generates more higher intensity speckles and worsens the uniformity of intensity in the overlapping beams.

As discussed above, two overlapping high intensity beams can couple to each other via their beat wave. This coupling process

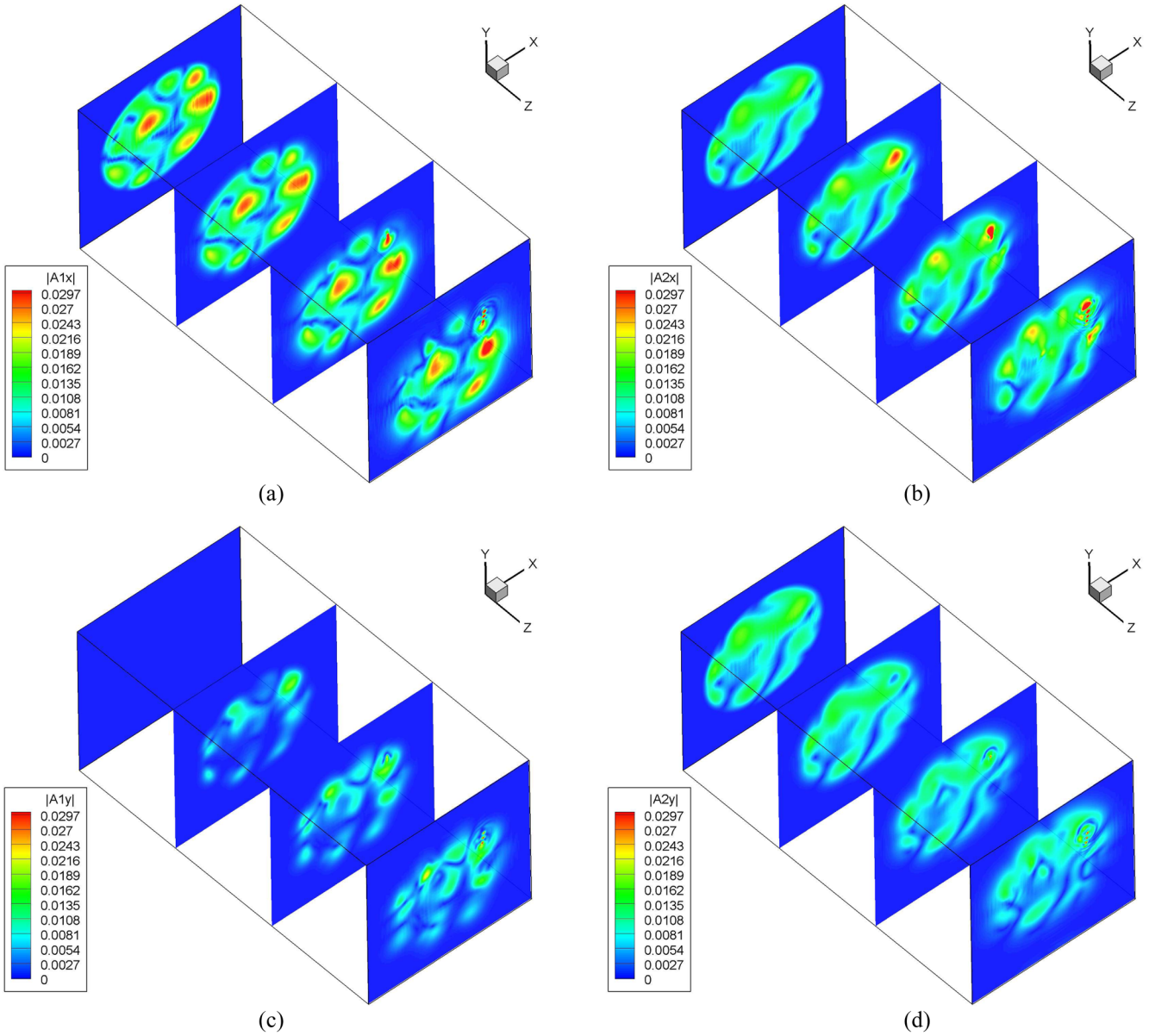

FIG. 4. Normalized absolute amplitude of the x [(a) and (b)] and y [(c) and (d)] polarization components of the vector potential on different slices in the $\hat{x}$–$\hat{y}$ plane at $z = 0\lambda_c$, $170\lambda_c$, $340\lambda_c$, and $512\lambda_c$ for beams 1 [(a) and (c)] and 2 [(b) and (d)] in case III.

is related to the phase velocity of the beat wave in the reference frame of the plasma, and the phase velocity is determined by the crossing angle and the wavelength separation between the two beams. In Fig. 3, we present the real and imaginary parts of the complex plasma coupling coefficient K as functions of the wavelength separation in the absence of plasma flow. When the two beams have the same wavelength, the imaginary part of K is zero, and so energy transfer between the two beams is prohibited. However, the real part of K is nonzero and induces a phase modulation of each laser beam. If we focus on the coupling term of the overlapping incident beams and ignore the terms in Eq. (4) associated with damping, refraction, diffraction, and SBS coupling, then, on substituting Eq. (8) into Eq. (4), we have

$$\frac{\partial A_{\alpha x}}{\partial z} = iK\frac{\omega_{pe}^2(k_\alpha - k_\beta)^2}{32\pi n_e m_e k_\alpha c^4}\left|A_{\beta x}\right|^2 A_{\alpha x}. \tag{10}$$

According to Eq. (10), the modulated phase of beam α ($\alpha = 1, 2$) is proportional to the local intensity of beam β ($\beta = 2, 1$). For a laser beam spot smoothed by a CPP, there are many speckles with

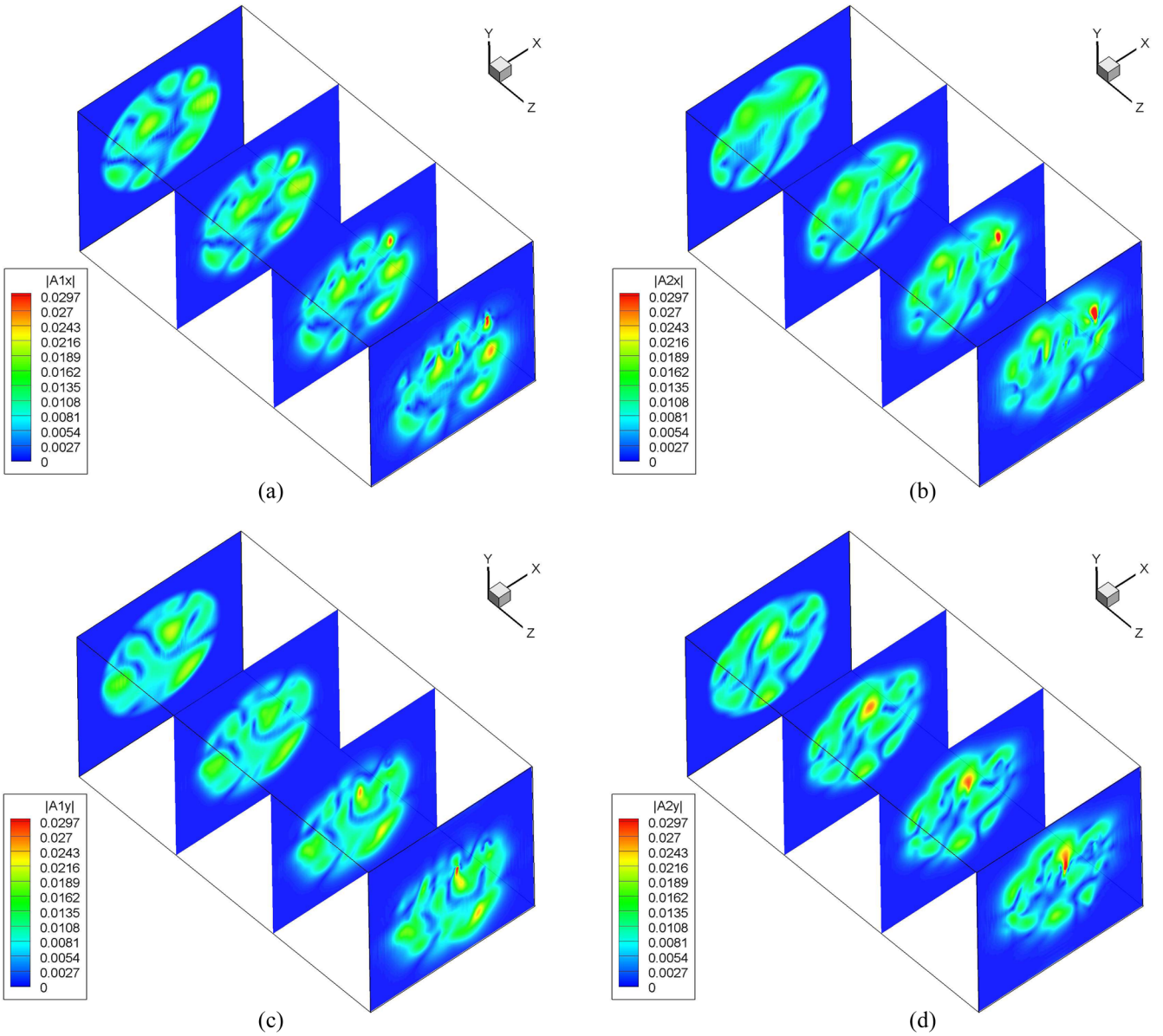

FIG. 5. Normalized absolute amplitude of the x [(a) and (b)] and y [(c) and (d)] polarization components of the vector potential on different slices in the $\hat{x}$–$\hat{y}$ plane at $z = 0\lambda_c$, $170\lambda_c$, $340\lambda_c$, and $512\lambda_c$ for beams 1 [(a) and (c)] and 2 [(b) and (d)] in case IV.

full-width half-maximum transverse length about $F\lambda_c$ located at different positions within the beam spot, where F is the F-number of the laser beam.[40] Therefore, the intensity distribution on each wavefront plane is nonuniform within the beam spot, which means that the modulated phase is also nonuniform on the wavefront plane for the overlapping beams. As is well known, the amplitude of the vector potential on the wavefront plane is the superposition of the light transmitted from the former wavefront plane. After the nonuniform phase has been added to the complex amplitude of the vector potential on a given wavefront plane, the intensity distribution will be changed in the following wavefront plane, and this change is greater near the overlapping region of the high intensity speckles of the two laser beams, as shown in Fig. 1. Besides, the amplitude of the laser light at each point on the following wavefront plane can be either increased or decreased by the superposition. As a result, within a speckle generated by the CPP, the laser intensity will become higher at some positions but lower at others. That is the speckles generated by the CPP are broken into a greater number of smaller speckles with higher intensities, as indicated by the small high intensity points shown in Figs. 1(c) and 1(d). If the overlapping region of the speckles is long enough, the smaller speckles will be split again in a similar way, which will further result in filamentations in the overlapping laser beams. As indicated by the differences revealed in Figs. 1(e) and 1(f), the coupling of high intensity overlapping beams can result in speckle splitting and even filamentation at low density, as long as the wavelength separation is in the range of $\mathrm{Re}(K) \neq 0$.

To investigate the influence of polarization on the coupling of overlapping beams, we perform a simulation with two laser beams whose polarizations are at an angle of 45°. In case III, the polarization of beam 1 is kept in the x direction, while the polarization of beam 2 is set at 45° in the $\hat{x}$–$\hat{y}$ plane with the same intensity. Figures 4(a) and 4(c) show the polarization components in the x and y directions of beam 1 (A_{1x} and A_{1y}) in different $\hat{x}$–$\hat{y}$ slices, while the two polarization components of beam 2 (A_{2x} and A_{2y}) are presented in Figs. 4(b) and 4(d). In the incident plane, A_{1y} is zero and the two polarization components of beam 2 are the same. Because of the coupling of the overlapping beams, as the two laser beams propagate, A_{1y} gradually increases and the average intensities of the two polarization components of beam 2 are no longer equal. Although there is no incident source of A_{1y}, the first term on the right-hand side of Eq. (5) is nonzero, and so the coupling induces the polarization component A_{1y} of beam 1 in the $\hat{x}$–$\hat{y}$ plane.[38] Because the modulated phase is nonuniform, the polarization components of $\vec{A}_1$ are not distributed uniformly in space. Similarly, the polarization components of $\vec{A}_2$ also vary in space. Furthermore, the intensity distribution in the $\hat{x}$–$\hat{y}$ plane changes significantly for the two polarization components along the $\hat{z}$ direction. We define the intensity fraction as

$$f_{\alpha i}(z) = \frac{\left\langle |A_{\alpha i}(x,y,z)|^2 \right\rangle_{x,y}}{\sum_i \left\langle |A_{\alpha i}(x,y,0)|^2 \right\rangle_{x,y}}, \tag{11}$$

where $\alpha = 1, 2$ and $i = x, y$. In the outgoing plane, the diagnosed $f_{1x}(512\lambda_c) = 39.5\%$ and $f_{1y}(512\lambda_c) = 10.5\%$ for beam 1, and $f_{2x}(512\lambda_c) = 35.5\%$ and $f_{2y}(512\lambda_c) = 14.5\%$ for beam 2. Thus, the total intensity fraction of the two beams in the x direction, $f_{1x}(512\lambda_c) + f_{2x}(512\lambda_c) = f_{1x}(0) + f_{2x}(0) = 75\%$, remains unchanged, as does the total intensity fraction in the y direction, $f_{1y}(512\lambda_c) + f_{2y}(512\lambda_c)$. Furthermore, owing to the nonuniformity of the phase coupling in space, some high intensity speckles are also

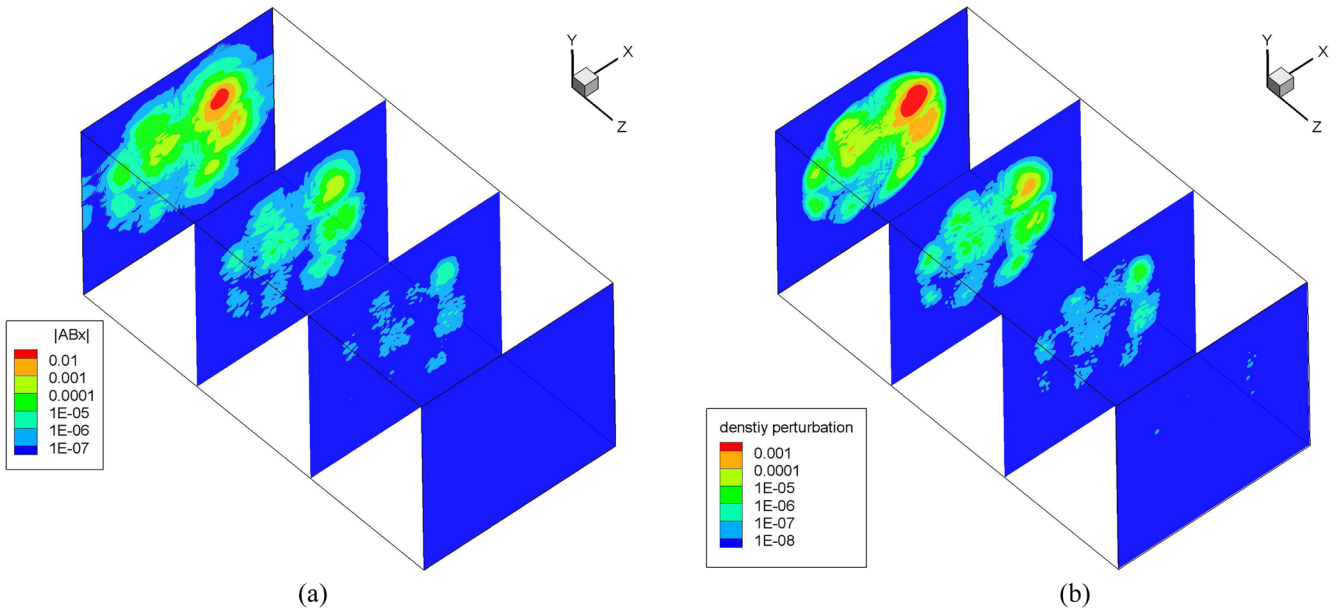

FIG. 6. (a) Normalized absolute amplitude of the vector potential on different slices in the $\hat{x}$–$\hat{y}$ plane at $z = 0\lambda_c$, $170\lambda_c$, $340\lambda_c$, and $512\lambda_c$ for scattered light from SBS in case II. (b) Normalized absolute amplitude of the density perturbation on different slices in the $\hat{x}$–$\hat{y}$ plane at $z = 0\lambda_c$, $170\lambda_c$, $340\lambda_c$, and $512\lambda_c$ corresponding to the ion-acoustic wave stimulated by beam 2 in case II.

formed within the beam spots in the two polarization directions, as shown in Fig. 4. The FOPAI curves of the two polarization components of beams 1 and 2 in the outgoing plane are shown in Fig. 2, and it can be seen that the fraction of high intensity in the x polarization of the two beams in case III is higher than that in case I, which is consistent with the intensity distribution shown in Fig. 4.

The PS technique can be used to reduce the coupling between two overlapping beams, but it cannot eliminate it completely. In case IV, we consider the situation where two overlapping laser beams are smoothed by a CPP and PS simultaneously. As shown in Fig. 5, the distribution of speckles of $A_{\alpha x}$ and $A_{\alpha y}$ on the incident plane are not the same for each beam, owing to the speckle separation effect of the PS technique.[27] Thus, the coupling between the two overlapping beams is weakened compared with cases II and III. However, some overlapping of the speckles of the two beams in space is inevitable. Some small speckles with higher intensities are still formed owing to the nonuniform phase modulation, as shown in Fig. 5. As can be seen in Fig. 2, the fraction of high intensity on the outgoing plane in case IV is smaller than in case II and for the x polarization in case III, but the fraction of intensity near 3×10^{16} W/cm^2 in case IV is higher than in case I owing to the coupling of overlapping beams.

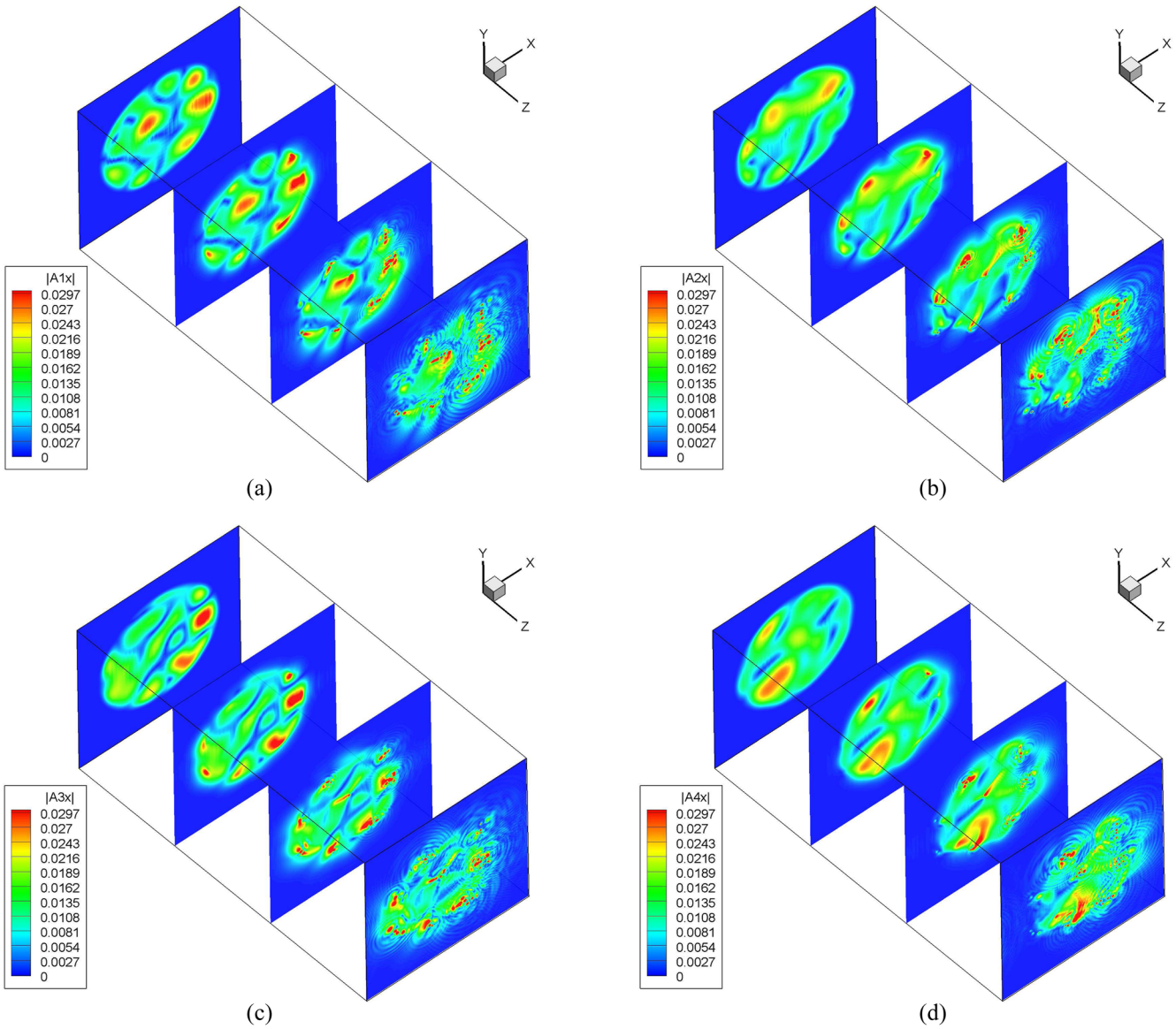

FIG. 7. Normalized absolute amplitude of the vector potential on different slices in the $\hat{x}$–$\hat{y}$ plane at $z = 0\lambda_c$, $170\lambda_c$, $340\lambda_c$, and $512\lambda_c$ for (a) beam 1, (b) beam 2, (c) beam 3, and (d) beam 4 in the case of four overlapping beams.

IV. INFLUENCE OF BEAM COUPLING ON SBS

Because LPIs are sensitive to laser intensity, the increase in high intensity speckles due to the coupling of overlapping beams might affect the growth of LPIs.[44] Taking SBS as an example, the growth of SBS is compared for the different laser conditions of the overlapping beams listed in Table I. In these simulations, seed light with random distribution in $\hat{k}_x$–$\hat{k}_y$ space is launched at the outgoing plane. The average intensity of this seed light is chosen as 1 kW/cm^2, which is a similar magnitude to the source from Thomson scattering.[45] The wavelength of the seed light is 351.515 nm, which optimally satisfies the matching condition for SBS here. Taking account of the possibility that the amplitude of the ion-acoustic wave might saturate owing to various nonlinear processes,[40] the density perturbations are limited by $0.05n_e$. Figure 6(a) shows the normalized amplitude of the SBS scattered light in case II in different slices in the $\hat{x}$–$\hat{y}$ plane. The corresponding amplitude of the density perturbation of the ion-acoustic wave stimulated by beam 2, which is normalized by the critical density, is shown in Fig. 6(b). The solution of Eqs. (4)–(9) in the three-dimensional simulation box for case II indicates that the SBS is stimulated by the two incident beams and grows mainly in a convective manner in the $-\hat{z}$ direction. Thus, the amplitudes of the SBS light and the corresponding ion-acoustic wave are largest in the incident plane for each line with the same coordinates (x, y). Because the convective growth of SBS will be higher in the superposition region of the high intensity speckles of the two beams, both the highest intensity of the scattered light and the density perturbations of the ion-acoustic wave are located in the right upper region on the incident plane, which is consistent with the spatial distribution of the superposed speckles with higher intensity on the $\hat{x}$–$\hat{y}$ plane shown in Figs. 1(c) and 1(d). The reflectivity of the SBS light on the incident plane in case II is enhanced about 1.6 times compared with that in case I. In case III, the reflectivity of the SBS light is close to that in case II and also much higher than that in case I. This indicates that adjusting the polarization angle of two overlapping beams would not reduce the coupling and the SBS significantly, except when the polarizations of the two beams are orthogonal. For overlapping beams smoothed by a CPP and PS simultaneously, coupling of the beams would still enhance the reflectivity of the SBS, because of the appearance of high intensity speckles.

V. ENHANCED COUPLING EFFECT FOR MULTIBEAM OVERLAPPING

The generation of high intensity speckles by the coupling of overlapping laser beams is enhanced when there are a greater number of overlapping beams. To show this effect, we perform a simulation with four overlapping laser beams. For convenience, beams 1 and 2 have the same incident conditions as in case II with two overlapping beams discussed above, and two additional beams smoothed by a CPP are launched at the incident plane with the same polarization direction. The incident angles of beams 3 and 4 are -2.5° and 2.5°, respectively, from the $\hat{z}$ axis in the x direction. Thus, the crossing angle between them is still 5°, while the crossing angle between beam 1 (or 2) and beam 3 (or 4) is about 3.54° symmetrically. The average intensity per beam is again 2×10^{15} W/cm^2. In this situation, the phase of each beam is modulated nonuniformly by the other three beams. Comparing Figs. 7(a) and 7(b) with Figs. 1(a) and 1(b), it can be seen that there are many more smaller speckles with higher intensities within each beam than in case II, owing to the coupling of the multiple beams. Statistically, the fraction of intensity higher than 2.5×10^{16} W/cm^2 diagnosed on the outgoing plane per beam is much higher than in case II, as shown in Fig. 8. The reflectivity of the SBS stimulated by the four overlapping beams is about 23% when beam coupling is considered, which is much higher than the 9.7% for four beams without coupling. Therefore, there will be greater generation of high intensity speckles due to coupling as the number of overlapping beams increases.

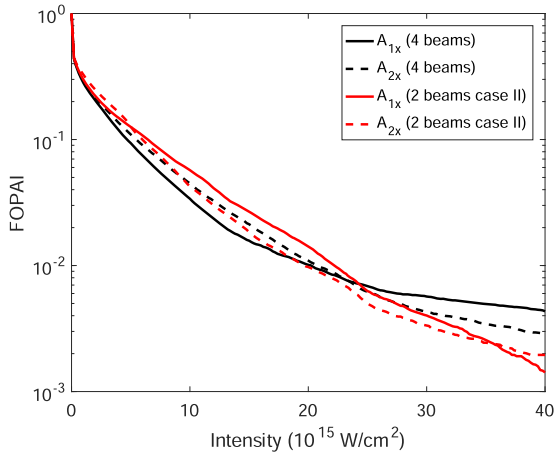

FIG. 8. FOPAI of beams 1 and 2 (solid and dashed lines, respectively) diagnosed in the outgoing $\hat{x}$–$\hat{y}$ plane. The red curves are for case II of two beams and the black curves for the case of four overlapping beams.

VI. DISCUSSION AND SUMMARY

A new mechanism for the generation of speckles with higher intensities due to the coupling of overlapping beams has been investigated thoroughly and verified through three-dimensional simulations. The simulation results show that the intensity distribution within each beam spot can be changed significantly by nonuniform spatial phase modulation, and the speckles are split into smaller ones with higher intensities. The coupling becomes stronger as the number of overlapping beams increases, and SBS is enhanced owing to the appearance of the higher intensity speckles. In direct-drive ICF, this mechanism may affect capsule implosion owing to laser imprinting. To exclude energy transfer between the incident beams and reveal the influence of the phase modulation clearly, the wavelength difference between the laser beams and the plasma flow velocity are both set to zero in our simulations. In reality, the flow velocity will induce a Doppler shift and offset the K value against the wavelength separation. However, our conclusions will remain valid as long as the real part of K is nonzero. It should be pointed out that the current wave-coupling model of COLA does not include nonlinearities such as ion trapping, two-ion wave decay, ion-acoustic wave harmonics, and ion-wave bowing,[46–50] which might be important if the number of speckles with higher intensities is increased greatly. Such nonlinear processes in overlapping beams will be investigated further in the future.

ACKNOWLEDGMENTS

This work was supported by the National Natural Science Foundation of China (Grant Nos. 12275032, 12035002, and 12205021) and the Project supported by CAEP Foundation (Grant No. CX20210040).

AUTHOR DECLARATIONS

Conflict of Interest

The authors have no conflicts to disclose.

Author Contributions

Liang Hao: Conceptualization (lead); Data curation (lead); Formal analysis (lead); Funding acquisition (equal); Investigation (lead); Methodology (equal); Software (lead); Visualization (lead); Writing – original draft (lead). **Jie Qiu**: Methodology (equal); Validation (lead); Writing – review & editing (supporting). **W. Y. Huo**: Conceptualization (supporting); Funding acquisition (equal); Project administration (lead); Supervision (lead); Writing – original draft (supporting); Writing – review & editing (lead).

DATA AVAILABILITY

The data that support the findings of this study are available from the corresponding author upon reasonable request.

REFERENCES

[1]E. M. Campbell, V. N. Goncharov, T. C. Sangster, S. P. Regan, P. B. Radha, R. Betti, J. F. Myatt, D. H. Froula, M. J. Rosenberg, I. V. Igumenshchev, W. Seka, A. A. Solodov, A. V. Maximov, J. A. Marozas, T. J. B. Collins, D. Turnbull, F. J. Marshall, A. Shvydky, J. P. Knauer, R. L. McCrory, A. B. Sefkow, M. Hohenberger, P. A. Michel, T. Chapman, L. Masse, C. Goyon, S. Ross, J. W. Bates, M. Karasik, J. Oh, J. Weaver, A. J. Schmitt, K. Obenschain, S. P. Obenschain, S. Reyes, and B. Van Wonterghem, "Laser-direct-drive program: Promise, challenge, and path forward," Matter Radiat. Extremes **2**(2), 37–54 (2017).

[2]J. D. Lindl, *Inertial Confinement Fusion: The Quest for Ignition and Energy Gain Using Indirect Drive* (Springer-Verlag, New York, 1998).

[3]K. B. Wharton, R. K. Kirkwood, S. H. Glenzer, K. G. Estabrook, B. B. Afeyan, B. I. Cohen, J. D. Moody, and C. Joshi, "Observation of energy transfer between identical-frequency laser beams in a flowing plasma," Phys. Rev. Lett. **81**(11), 2248–2251 (1998).

[4]P. Michel, S. H. Glenzer, L. Divol, D. K. Bradley, D. Callahan, S. Dixit, S. Glenn, D. Hinkel, R. K. Kirkwood, J. L. Kline, W. L. Kruer, G. A. Kyrala, S. Le Pape, N. B. Meezan, R. Town, K. Widmann, E. A. Williams, B. J. MacGowan, J. Lindl, and L. J. Suter, "Symmetry tuning via controlled crossed-beam energy transfer on the National Ignition Facility," Phys. Plasmas **17**, 056305 (2010).

[5]P. Michel, L. Divol, R. P. J. Town, M. D. Rosen, D. A. Callahan, N. B. Meezan, M. B. Schneider, G. A. Kyrala, J. D. Moody, E. L. Dewald, K. Widmann, E. Bond, J. L. Kline, C. A. Thomas, S. Dixit, E. A. Williams, D. E. Hinkel, R. L. Berger, O. L. Landen, M. J. Edwards, B. J. MacGowan, J. D. Lindl, C. Haynam, L. J. Suter, S. H. Glenzer, and E. Moses, "Three-wavelength scheme to optimize hohlraum coupling on the National Ignition Facility," Phys. Rev. E **83**, 046409 (2011).

[6]A. L. Kritcher, A. B. Zylstra, D. A. Callahan, O. A. Hurricane, C. Weber, J. Ralph, D. T. Casey, A. Pak, K. Baker, B. Bachmann, S. Bhandarkar, J. Biener, R. Bionta, T. Braun, M. Bruhn, C. Choate, D. Clark, J. M. Di Nicola, L. Divol, T. Doeppner, V. Geppert-Kleinrath, S. Haan, J. Heebner, V. Hernandez, D. Hinkel, M. Hohenberger, H. Huang, C. Kong, S. Le Pape, D. Mariscal, E. Marley, L. Masse, K. D. Meaney, M. Millot, A. Moore, K. Newman, A. Nikroo, P. Patel, L. Pelz, N. Rice, H. Robey, J. S. Ross, M. Rubery, J. Salmonson, D. Schlossberg, S. Sepke, K. Sequoia, M. Stadermann, D. Strozzi, R. Tommasini, P. Volegov, C. Wild, S. Yang, C. Young, M. J. Edwards, O. Landen, R. Town, and M. Herrmann, "Achieving record hot spot energies with large HDC implosions on NIF in HYBRID-E," Phys. Plasmas **28**, 072706 (2021).

[7]I. V. Igumenshchev, D. H. Edgell, V. N. Goncharov, J. A. Delettrez, A. V. Maximov, J. F. Myatt, W. Seka, A. Shvydky, S. Skupsky, and C. Stoeckl, "Crossed-beam energy transfer in implosion experiments on OMEGA," Phys. Plasmas **17**, 122708 (2010).

[8]J. Qiu, L. Hao, L. H. Cao, and S. Y. Zou, "Collective stimulated Brillouin scattering with shared ion acoustic wave under the action of two overlapping laser beams," Plasma Phys. Controlled Fusion **63**, 125026 (2021).

[9]D. Turnbull, P. Michel, J. E. Ralph, L. Divol, J. S. Ross, L. F. Berzak Hopkins, A. L. Kritcher, D. E. Hinkel, and J. D. Moody, "Multibeam seeded Brillouin sidescatter in inertial confinement fusion experiments," Phys. Rev. Lett. **114**, 125001 (2015).

[10]J. Qiu, L. Hao, L. H. Cao, and S. Y. Zou, "Collective stimulated Brillouin scattering modes of two crossing laser beams with shared scattered wave," Matter Radiat. Extremes **6**, 065903 (2021).

[11]Q. S. Feng, Z. J. Liu, L. H. Cao, C. Z. Xiao, L. Hao, C. Y. Zheng, C. Ning, and X. T. He, "Interaction of parametric instabilities from 3ω and 2ω lasers in large-scale inhomogeneous plasmas," Nucl. Fusion **60**, 066012 (2020).

[12]C. Z. Xiao, H. B. Zhuo, Y. Yin, Z. J. Liu, C. Y. Zheng, and X. T. He, "Linear theory of multibeam parametric instabilities in homogeneous plasmas," Phys. Plasmas **26**, 062109 (2019).

[13]Y. Zhao, C. F. Wu, S. M. Weng, Z. M. Sheng, and J. Q. Zhu, "Mitigation of multibeam stimulated Raman scattering with polychromatic light," Plasma Phys. Controlled Fusion **63**, 055006 (2021).

[14]S. Depierreux, C. Neuville, V. Tassin, M.-C. Monteil, P.-E. Masson-Laborde, C. Baccou, P. Fremerye, F. Philippe, P. Seytor, D. Teychenné, J. Katz, R. Bahr, M. Casanova, N. Borisenko, L. Borisenko, A. Orekhov, A. Colaitis, A. Debayle, G. Duchateau, A. Heron, S. Huller, P. Loiseau, P. Nicolai, C. Riconda, G. Tran, C. Stoeckl, W. Seka, V. Tikhonchuk, D. Pesme, and C. Labaune, "Experimental investigation of the collective stimulated Brillouin and Raman scattering of multiple laser beams in inertial confinement fusion experiments," Plasma Phys. Controlled Fusion **62**, 014024 (2020).

[15]J. Qiu, L. Hao, L. H. Cao, and S. Y. Zou, "Investigation of Langdon effect on the stimulated backward Raman and Brillouin scattering," Plasma Phys. Controlled Fusion **63**, 125021 (2021).

[16]L. Hao, W. Y. Huo, Z. J. Liu, J. Li, C. Y. Zheng, and C. Ren, "A frequency filter of backscattered light of stimulated Raman scattering due to the Raman rescattering in the gas-filled hohlraums," Nucl. Fusion **61**, 036041 (2021).

[17]Y. Ji, C.-W. Lian, R. Yan, C. Ren, D. Yang, Z.-H. Wan, B. Zhao, C. Wang, Z.-H. Fang, and J. Zheng, "Convective amplification of stimulated Raman rescattering in a picosecond laser plasma interaction regime," Matter Radiat. Extremes **6**, 015901 (2021).

[18]J. Qiu, L. Hao, L. H. Cao, and S. Y. Zou, "Investigation of the Langdon effect on the nonlinear evolution of SRS from the early-stage inflation to the late-stage development of secondary instabilities," Nucl. Fusion **62**, 126072 (2022).

[19]J. F. Myatt, J. Zhang, R. W. Short, A. V. Maximov, W. Seka, D. H. Froula, D. H. Edgell, D. T. Michel, I. V. Igumenshchev, D. E. Hinkel, P. Michel, and J. D. Moody, "Multiple-beam laser-plasma interactions in inertial confinement fusion," Phys. Plasmas **21**, 055501 (2014).

[20]V. Tikhonchuk, Y. J. Gu, O. Klimo, J. Limpouch, and S. Weber, "Studies of laser-plasma interaction physics with low-density targets for direct-drive inertial confinement schemes," Matter Radiat. Extremes **4**, 045402 (2019).

[21]A. L. Kritcher, A. B. Zylstra, D. A. Callahan, O. A. Hurricane, C. R. Weber, D. S. Clark, C. V. Young, J. E. Ralph, D. T. Casey, A. Pak, O. L. Landen, B. Bachmann, K. L. Baker, L. Berzak Hopkins, S. D. Bhandarkar, J. Biener, R. M. Bionta, N. W. Birge, T. Braun, T. M. Briggs, P. M. Celliers, H. Chen, C. Choate, L. Divol, T. Döppner, D. Fittinghoff, M. J. Edwards, M. Gatu Johnson, N. Gharibyan, S. Haan, K. D. Hahn, E. Hartouni, D. E. Hinkel, D. D. Ho, M. Hohenberger, J. P. Holder, H. Huang, N. Izumi, J. Jeet, O. Jones, S. M. Kerr, S. F. Khan, H. Geppert Kleinrath, V. Geppert Kleinrath, C. Kong, K. M. Lamb, S. Le Pape, N. C. Lemos, J. D. Lindl, B. J. MacGowan, A. J. Mackinnon, A. G. MacPhee, E. V. Marley, K. Meaney, M. Millot, A. S. Moore, K. Newman, J. G. Di Nicola, A. Nikroo, R. Nora, P. K. Patel, N. G. Rice, M. S. Rubery, J. Sater, D. J. Schlossberg, S. M. Sepke, K. Sequoia, S. J. Shin, M. Stadermann, S. Stoupin, D. J. Strozzi, C. A. Thomas, R. Tommasini, C. Trosseille, E. R. Tubman, P. L. Volegov, C. Wild,

D. T. Woods, and S. T. Yang, "Design of an inertial fusion experiment exceeding the Lawson criterion for ignition," Phys. Rev. E **106**, 025201 (2022).
[22]A. B. Zylstra, A. L. Kritcher, O. A. Hurricane, D. A. Callahan, J. E. Ralph, D. T. Casey, A. Pak, O. L. Landen, B. Bachmann, K. L. Baker, L. Berzak Hopkins, S. D. Bhandarkar, J. Biener, R. M. Bionta, N. W. Birge, T. Braun, T. M. Briggs, P. M. Celliers, H. Chen, C. Choate, D. S. Clark, L. Divol, T. Döppner, D. Fittinghoff, M. J. Edwards, M. Gatu Johnson, N. Gharibyan, S. Haan, K. D. Hahn, E. Hartouni, D. E. Hinkel, D. D. Ho, M. Hohenberger, J. P. Holder, H. Huang, N. Izumi, J. Jeet, O. Jones, S. M. Kerr, S. F. Khan, H. Geppert Kleinrath, V. Geppert Kleinrath, C. Kong, K. M. Lamb, S. Le Pape, N. C. Lemos, J. D. Lindl, B. J. MacGowan, A. J. Mackinnon, A. G. MacPhee, E. V. Marley, K. Meaney, M. Millot, A. S. Moore, K. Newman, J. G. Di Nicola, A. Nikroo, R. Nora, P. K. Patel, N. G. Rice, M. S. Rubery, J. Sater, D. J. Schlossberg, S. M. Sepke, K. Sequoia, S. J. Shin, M. Stadermann, S. Stoupin, D. J. Strozzi, C. A. Thomas, R. Tommasini, C. Trosseille, E. R. Tubman, P. L. Volegov, C. R. Weber, C. Wild, D. T. Woods, S. T. Yang, and C. V. Young, "Experimental achievement and signatures of ignition at the National Ignition Facility," Phys. Rev. E **106**, 025202 (2022).
[23]Y. Kato, K. Mima, N. Miyanaga, S. Arinaga, Y. Kitagawa, M. Nakatsuka, and C. Yamanaka, "Random phasing of high-power lasers for uniform target acceleration and plasma-instability suppression," Phys. Rev. Lett. **53**, 1057 (1984).
[24]S. N. Dixit, J. K. Lawson, K. R. Manes, H. T. Powell, and K. A. Nugent, "Kinoform phase plates for focal plane irradiance profile control," Opt. Lett. **19**, 417–419 (1994).
[25]A. Le Cain, G. Riazuelo, and J. M. Sajer, "Statistical spatio-temporal properties of the Laser MegaJoule speckle," Phys. Plasmas **19**, 102704 (2012).
[26]S. Skupsky, R. W. Short, T. Kessler, R. S. Craxton, S. Letzring, and J. M. Soures, "Improved laser-beam uniformity using the angular dispersion of frequency-modulated light," J. Appl. Phys. **66**, 3456 (1989).
[27]D. H. Froula, L. Divol, R. L. Berger, R. A. London, N. B. Meezan, D. J. Strozzi, P. Neumayer, J. S. Ross, S. Stagnitto, L. J. Suter, and S. H. Glenzer, "Direct measurements of an increased threshold for stimulated Brillouin scattering with polarization smoothing in ignition hohlraum plasmas," Phys. Rev. Lett. **101**, 115002 (2008).
[28]B. J. Albright, L. Yin, and B. Afeyan, "Control of stimulated Raman scattering in the strongly nonlinear and kinetic regime using spike trains of uneven duration and delay," Phys. Rev. Lett. **113**, 045002 (2014).
[29]I. Barth and N. J. Fisch, "Reducing parametric backscattering by polarization rotation," Phys. Plasmas **23**, 102106 (2016).
[30]Y. Zhao, S. M. Weng, M. Chen, J. Zheng, H. B. Zhuo, and Z. M. Sheng, "Stimulated Raman scattering excited by incoherent light in plasma," Matter Radiat. Extremes **2**, 190 (2017).
[31]J. W. Bates, J. F. Myatt, J. G. Shaw, R. K. Follett, J. L. Weaver, R. H. Lehmberg, and S. P. Obenschain, "Mitigation of cross-beam energy transfer in inertial-confinement-fusion plasmas with enhanced laser bandwidth," Phys. Rev. E **97**, 061202(R) (2018).
[32]Z. Q. Zhong, B. Li, H. Xiong, J. W. Li, J. Qiu, L. Hao, and B. Zhang, "Effective optical smoothing scheme to suppress laser plasma instabilities by time-dependent polarization rotation via pulse chirping," Opt. Express **29**(2), 1304 (2021).
[33]H. H. Ma, X. F. Li, S. M. Weng, S. H. Yew, S. Kawata, P. Gibbon, Z. M. Sheng, and J. Zhang, "Mitigating parametric instabilities in plasmas by sunlight-like lasers," Matter Radiat. Extremes **6**, 055902 (2021).
[34]S. Kawata, "Dynamic mitigation of instabilities," Phys. Plasmas **19**, 024503 (2012).
[35]S. Kawata, Y. J. Gu, X. F. Li, T. Karino, H. Katoh, J. Limpouch, O. Klimo, D. Margarone, Q. Yu, Q. Kong, S. Weber, S. Bulanov, and A. Andreev, "Dynamic stabilization of filamentation instability," Phys. Plasmas **25**, 011601 (2018).
[36]Y. Q. Gao, Y. Cui, L. J. Ji, D. X. Rao, X. H. Zhao, F. J. Li, D. Liu, W. Feng, L. Xia, J. N. Liu, H. T. Shi, P. Y. Du, J. Liu, X. L. Li, T. Wang, T. X. Zhang, C. Shan, Y. L. Hua, W. X. Ma, X. Sun, X. F. Chen, X. G. Huang, J. Zhu, W. B. Pei, Z. Sui, and S. Z. Fu, "Development of low-coherence high-power laser drivers for inertial confinement fusion," Matter Radiat. Extremes **5**, 065201 (2020).
[37]D. Turnbull, C. Goyon, G. E. Kemp, B. B. Pollock, D. Mariscal, L. Divol, J. S. Ross, S. Patankar, J. D. Moody, and P. Michel, "Refractive index seen by a probe beam interacting with a laser-plasma system," Phys. Rev. Lett. **118**, 015001 (2017).
[38]P. Michel, L. Divol, D. Turnbull, and J. D. Moody, "Dynamic control of the polarization of intense laser beams via optical wave mixing in plasmas," Phys. Rev. Lett. **113**, 205001 (2014).
[39]P. Michel, E. Kur, M. Lazarow, T. Chapman, L. Divol, and J. S. Wurtele, "Polarization-dependent theory of two-wave mixing in nonlinear media, and application to dynamical polarization control," Phys. Rev. X **10**, 021039 (2020).
[40]R. L. Berger, C. H. Still, E. A. Williams, and A. B. Langdon, "On the dominant and subdominant behavior of stimulated Raman and Brillouin scattering driven by nonuniform laser beams," Phys. Plasmas **5**, 4337 (1998).
[41]B. D. Fried and S. D. Conte, *The Plasma Dispersion Function: The Hilbert Transform of the Gaussian* (Academic, New York, 1961).
[42]T. Gong, L. Hao, Z. C. Li, D. Yang, S. W. Li, X. Li, L. Guo, S. Y. Zou, Y. Y. Liu, X. H. Jiang, X. S. Peng, T. Xu, X. M. Liu, Y. L. Li, C. Y. Zheng, H. B. Cai, Z. J. Liu, J. Zheng, Z. B. Wang, Q. Li, P. Li, R. Zhang, Y. Zhang, F. Wang, D. Wang, F. Wang, S. Y. Liu, J. M. Yang, S. E. Jiang, B. H. Zhang, and Y. K. Ding, "Recent research progress of laser plasma interactions in Shenguang laser facilities," Matter Radiat. Extremes **4**, 055202 (2019).
[43]P. Loiseau, P.-E. Masson-Laborde, D. Teychenné, M.-C. Monteil, M. Casanova, D. Marion, G. Tran, G. Huser, C. Rousseaux, S. Hüller, A. Héron, and D. Pesme, "Simulation of laser-plasma interaction experiments with gas-filled hohlraums on the LIL facility," J. Phys.: Conf. Ser. **688**, 012059 (2016).
[44]V. T. Tikhonchuk, T. Gong, N. Jourdain, O. Renner, F. P. Condamine, K. Q. Pan, W. Nazarov, L. Hudec, J. Limpouch, R. Liska, M. Krůs, F. Wang, D. Yang, S. W. Li, Z. C. Li, Z. Y. Guan, Y. G. Liu, T. Xu, X. S. Peng, X. M. Liu, Y. L. Li, J. Li, T. M. Song, J. M. Yang, S. E. Jiang, B. H. Zhang, W. Y. Huo, G. Ren, Y. H. Chen, W. Zheng, Y. K. Ding, K. Lan, and S. Weber, "Studies of laser-plasma interaction physics with low-density targets for direct-drive inertial confinement fusion on the Shenguang III prototype," Matter Radiat. Extremes **6**, 025902 (2021).
[45]T. Gong, Z. C Li, B. Zhao, G. Y. Hu, and J. Zheng, "Noise sources and competition between stimulated Brillouin and Raman scattering: A one-dimensional steady-state approach," Phys. Plasmas **20**, 092702 (2013).
[46]A. G. Seaton, L. Yin, R. K. Follett, B. J. Albright, and A. Le, "Cross-beam energy transfer in direct-drive ICF. I. Nonlinear and kinetic effects," Phys. Plasmas **29**, 042706 (2022).
[47]C. Niemann, S. H. Glenzer, J. Knight, L. Divol, E. A. Williams, G. Gregori, B. I. Cohen, C. Constantin, D. H. Froula, D. S. Montgomery, and R. P. Johnson, "Observation of the parametric two-ion decay instability with Thomson scattering," Phys. Rev. Lett. **93**, 045004 (2004).
[48]B. J. Albright, L. Yin, K. J. Bowers, and B. Bergen, "Multi-dimensional dynamics of stimulated Brillouin scattering in a laser speckle: Ion acoustic wave bowing, breakup, and laser-seeded two-ion-wave decay," Phys. Plasmas **23**, 032703 (2016).
[49]Q. S. Feng, L. H. Cao, Z. J. Liu, L. Hao, C. Y. Zheng, C. Ning, and X. T. He, "Growth rate and gain of stimulated Brillouin scattering considering nonlinear Landau damping due to particle trapping," Plasma Phys. Controlled Fusion **62**, 045013 (2020).
[50]Q. S. Feng, C. Y. Zheng, Z. J. Liu, L. H. Cao, C. Z. Xiao, Q. Wang, H. C. Zhang, and X. T. He, "Harmonic effects on ion-bulk waves and simulation of stimulated ion-bulk-wave scattering in CH plasmas," Plasma Phys. Controlled Fusion **59**, 085007 (2017).